Journal of Power Sources 225 (2013) 172–178

Contents lists available at SciVerse ScienceDirect

Journal of Power Sources

journal homepage: www.elsevier.com/locate/jpowsour

The effect of different binders on electrochemical properties of $LiNi_{1/3}Mn_{1/3}Co_{1/3}O_2$ cathode material in lithium ion batteries

Jiantie Xu [a], Shu-Lei Chou [a,*], Qin-fen Gu [b], Hua-Kun Liu [a], Shi-Xue Dou [a]

[a] Institute for Superconducting and Electronic Materials, University of Wollongong, Wollongong NSW 2522, Australia
[b] Australian Synchrotron, 800 Blackburn Rd, Clayton 3168, Australia

HIGHLIGHTS

- Three type of binders CMC, PVDF, and alginate were investigated for $LiNi_{1/3}Mn_{1/3}Co_{1/3}O_2$ (NMC).
- The electrode using CMC as a binder shows the best high rate capability.
- The electrode using CMC as a binder shows the lowest apparent activation energy.
- CMC could be the next generation cheap and green binder for NMC materials.

ARTICLE INFO

Article history:
Received 3 July 2012
Received in revised form
19 September 2012
Accepted 12 October 2012
Available online 22 October 2012

Keywords:
Lithium ion battery
Cathode materials
Binder
Sodium carboxylmethyl cellulose
Alginate

ABSTRACT

$LiNi_{1/3}Mn_{1/3}Co_{1/3}O_2$ (NMC) as a cathode material for lithium ion batteries has been synthesized by the sol–gel method. The X-ray diffraction Rietveld refinement results indicated that single-phase NMC with hexagonal layered structure was obtained. Scanning electron microscope images revealed well crystallized NMC with uniform particle size in the range of 100–200 nm. The performance of the NMC electrodes with sodium carboxylmethyl cellulose (CMC), poly(vinylidene fluoride) (PVDF), and alginate from brown algae as binders was compared. Constant current charge–discharge test results demonstrated that the NMC electrode using CMC as binder had the highest rate capability, followed by those using alginate and PVDF binders, respectively. Electrochemical impedance spectroscopy test results showed that the electrode using CMC as the binder had lower charge transfer resistance and lower apparent activation energy than the electrodes using alginate and PVDF as the binders. The apparent activation energies of NMC electrodes using CMC, alginate, and PVDF as binders were calculated to be 27.4 kJ mol^{-1}, 33.7 kJ mol^{-1}, and 36 kJ mol^{-1}, respectively.

1. Introduction

The lithium ion battery (LIB) is one of the most promising energy storage systems for portable computers, mobile devices, hybrid electric vehicles (HEVs), and plug-in hybrid electric vehicles [1]. There have been extensive studies on electrode materials, electrolytes, additives, membranes, and binders to achieve improvement of the battery performance [2]. Compared with the significant progress on most of these components for the lithium ion battery, however, binders for the lithium ion battery have not yet been as well investigated [3–5]. Although binders are electrochemically inactive materials, they can have a significant influence on the electrode performance. Currently, the organic solvent-based poly(vinylidene difluoride) (PVDF) has been widely used as the binder for both the negative and the positive electrodes in commercial LIBs, as a result of its good electrochemical stability and high adhesion to electrode materials and current collectors. Nonetheless, PVDF binder is expensive, not easily to recycle, and involved the use of volatile organic compounds such as the environmentally harmful and toxic *N*-methyl-2-pyrrolidone (NMP) for its processing [6,7]. Thus, to find cheap, environmentally friendly binders to substitute for the current commercial PVDF binder is important for the improvement of electrochemical performance and for decreasing the manufacturing costs of LIBs.

Carboxymethyl cellulose (CMC), which is produced from the insertion of carboxymethyl groups into natural cellulose, has recently attracted more consideration due to its ability to dissolve much more easily in water and its low cost compared with PVDF binder. Due to both apparent advantages, reports on the application of CMC as the binder for lithium ion batteries have demonstrated its

* Corresponding author. Tel.: +61 2 42981405; fax: +61 2 42215731.
E-mail addresses: shulei@uow.edu.au, sc478@uow.edu.au (S.-L. Chou).

0378-7753/$ – see front matter © 2012 Elsevier B.V. All rights reserved.
http://dx.doi.org/10.1016/j.jpowsour.2012.10.033

promising characteristics, such as its cycling stability, electrochemical capacity improvement, and environmental friendliness [8–11]. Very recently, alginate, which is a cheap, high-modulus natural polysaccharide extracted from brown algae, has been used as a binder mixed with Si anode, which presents even more remarkable electrochemical capacity improvement and cycling stability than CMC or PVDF binders [12]. Therefore, the diversity of binders and their advantages for lithium ion batteries can provide more opportunities to improve the energy densities of these batteries for successful commercial applications.

Although there have been more extensive investigations of the CMC and alginate binders in such anode materials as natural graphite [13], $LiTi_4O_{12}$ [14], SnO_2 [15,16], Fe_2O_3 [16,17], and Si [12,17–21], promising CMC and alginate binders to be used with cathode materials in lithium ion batteries are also ripe for investigation. To date, only very limited investigations of the effects of CMC on cathode materials have been carried out in comparison with different binders. Zaghib et al. revealed that ~2 wt% water-soluble elastomer binder (WSB) and ~2 wt% CMC blended with $LiFePO_4$ cathode material presented low irreversible capacity loss and stable cycling life [22]. Paik et al. reported the effects of CMC on aqueous processing of $LiFePO_4$ cathodes and their electrochemical performance [23,24]. Li et al. found that $Li[Li_{0.2}Mn_{0.56}Ni_{0.16}Co_{0.08}]O_2$ could perform well with CMC binder at very high voltages (4.8 V) in 1 M $LiPF_6$ in 1:1 ethylene carbonate: dimethyl carbonate (EC:DMC) solution as electrolyte [25]. Very recently, Wang et al. reported CMC as a binder in high voltage $LiNi_{0.4}Mn_{1.6}O_4$ cathode with close to the theoretical capacity (146 mAh g^{-1}) and low self-discharge (~10%) [26]. $LiNi_{1/3}Mn_{1/3}Co_{1/3}O_2$ (NMC), as one of the most promising large-scale commercial cathodes for lithium ion batteries, has shown its overwhelming advantages of high operating voltage, high specific capacity, cyclic stability, and structural stability [27–32]. However, there have been no reports on the use of CMC and alginate as binders in $LiNi_{1/3}Mn_{1/3}Co_{1/3}O_2$ cathode materials. Here, we study the effects of CMC and alginate binders on the electrochemical performance of $LiNi_{1/3}Mn_{1/3}Co_{1/3}O_2$ cathode material prepared by the sol–gel method for the first time.

2. Experimental

2.1. Synthesis

The $LiNi_{1/3}Mn_{1/3}Co_{1/3}O_2$ compound was prepared by the citric acid assisted sol–gel method. The starting materials CH_3COOLi, $Ni(CH_3COO)_2\cdot 6H_2O$, $Mn(CH_3COO)_2\cdot 4H_2O$, $Co(CH_3COO)_2\cdot 6H_2O$, and citric acid were dissolved in water to form a clear solution according to the ratio of Li:Ni:Mn:Co:citric acid = 3.15:1:1:1:3. The solution was heated gently with continuous stirring in a thermostatic water bath for several hours to remove the excess water at 80 °C until a pink solution formed. After drying it at 120 °C in air in an oven, the gel was put into an alumina boat and heated at 400 °C for 4 h under air to promote decomposition of the organic compounds. After cooling to room temperature, the precursor mixture was ground again and heated at 850 °C for 15 h under the same atmosphere to obtain the final dark powders. The $LiNi_{1/3}Mn_{1/3}Co_{1/3}O_2$–CMC material was obtained from the $LiNi_{1/3}Mn_{1/3}Co_{1/3}O_2$ material mixed with CMC binder in the water under different time duration. Then $LiNi_{1/3}Mn_{1/3}Co_{1/3}O_2$ was washed four times and dried in the vacuum oven under 80 °C.

2.2. Sample characterization

The phase identification of $LiNi_{1/3}Mn_{1/3}Co_{1/3}O_2$ compound was carried out using powder X-ray diffraction (XRD, GBC MMA 017). The phase of $LiNi_{1/3}Mn_{1/3}Co_{1/3}O_2$ and $LiNi_{1/3}Mn_{1/3}Co_{1/3}O_2$–CMC were identified by the Synchrotron X-ray diffraction from Powder diffraction beamline at Australian Synchrotron (Clayton, Australia), with a wavelength of 0.8260 Å. The morphology of the $LiNi_{1/3}Mn_{1/3}Co_{1/3}O_2$ compound was examined by a high resolution field emission scanning electron microscope (SEM; JEO: FESEM-7500, 30kv). The specific surface area was measured using 15 point N_2 absorption Brunauer–Emmett–Teller (BET) method using Quanta Chrome Nova 1000.

2.3. Electrochemical evaluation

The electrochemical characterization of the $LiNi_{1/3}Mn_{1/3}Co_{1/3}O_2$ compound was carried out using coin cells. The cathodes in the two-electrode electrochemical cells were fabricated by blending the NMC powders with acetylene black and different binders, including CMC, alginate, and PVDF binders, in a weight ratio of 85:10:5. It should be noted that de-ionised (DI) water was employed as the solvent for blending the electrode mixture for the CMC and alginate binders while *N*-methyl-2-pyrrolidone (NMP) was used as the blending solvent for the PVDF binder. The slurries were prepared using Kurabo MAZERUSTAR planetary mixer KK-250S for 15 min. The obtained slurry was coated on Al foil, dried at 90 °C for 12 h and pressed at the pressures of 2 MPa. The electrodes fabricated were dried again at 90 °C for 12 h in a vacuum after cutting into 1 cm × 1 cm in size where about 6 mg of active material were held. CR 2032 coin-type cells were assembled in an Ar-filled glove box by with Li foil as the counter electrode and reference electrode, a porous polypropylene film as separator, and 1 M $LiPF_6$ in a 1:2 (v/v) mixture of ethylene carbonate (EC) and diethylene carbonate (DEC) as the electrolyte. The cells were galvanostatically charged and discharged using an automatic battery tester system (Land®, China) at various current densities in the range of 2.5–4.6 V at room temperature and at current densities with various C-rates, with a theoretical specific capacity $C = 200$ mAh g^{-1}. Electrochemical impedance spectroscopy (EIS) measurements were performed on a Biologic MVP 3 electrochemical workstation over a frequency range of 10 mHz–1 MHz at the discharged stage of 3.7 V.

3. Results and discussions

Fig. 1 shows the X-ray diffraction (XRD) Rietveld refinement results for the as-prepared NMC. It can be seen that all peaks are very sharp, clear, and well-defined, suggesting that the as-prepared $LiNi_{1/3}Mn_{1/3}Co_{1/3}O_2$ is well crystallized. The well separated peaks, the Miller indices of which are indexed as (101), (106), and (102);

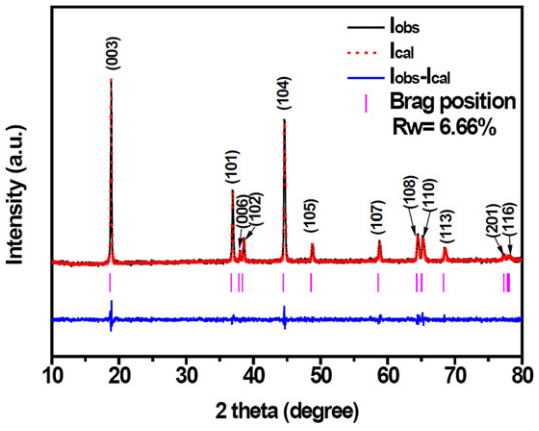

Fig. 1. XRD Rietveld refinement of $LiNi_{1/3}Mn_{1/3}Co_{1/3}O_2$.

and (108) and (110), respectively, indicate the highly ordered layer structure of $LiNi_{1/3}Mn_{1/3}Co_{1/3}O_2$. Typical layered structure type of α-$NaFeO_2$ with space group $R\bar{3}m$ was chosen as the refinement model. The reasonably small weighted profile *R*-factor, R_{wp}, (~6.66%) suggests that single-phase $LiNi_{1/3}Mn_{1/3}Co_{1/3}O_2$ has been well obtained. The lattice parameters of the NMC, which include *a*, *c*, *V*, and *c*/*a*, are very close to those previously reported [33] and are presented in Table 1. It should be noted that the high values of *c* and *c*/*a*, 14.25326(7) and 4.978, respectively, are beneficial to the formation of well-defined hexagonal layered structures. Furthermore, the integrated intensity ratio of $I_{(003)}/I_{(104)}$ was larger than 1.2, indicating a low degree of cation disorder in the structure because of the close ionic sizes of Li^+ (0.72Å) and Ni^{2+} (0.70Å).

Synchrotron powder X-Ray Diffraction (SXRD) was used to investigate any modification of the $LiNi_{1/3}Mn_{1/3}Co_{1/3}O_2$ materials after mixing with CMC binder in the water. The results from SXRD Rietveld refinement was shown in Fig. 2 and Table 1 There are no impurities and no significant impact on the crystal structure with the similar cell parameters of $LiNi_{1/3}Mn_{1/3}Co_{1/3}O_2$ (NMC), when NMC material was added into CMC water solution under different time duration. The cell parameters (*a*, *c* and *V*) values varied within the range of 0.05% compared to those for the pristine NMC, which is in the error range of refinement.

In addition, the ratio of $Li/Li_{pristine}$ ($Li_{pristine}$ = 1 for $LiNi_{1/3}Mn_{1/3}Co_{1/3}O_2$) vs. mixing time was shown in Fig. 2(c). The partial lithium lost could be found in the $LiNi_{1/3}Mn_{1/3}Co_{1/3}O_2$ samples mixing with CMC binder in the water. This is probably due to the exchange between Li^+ in $LiNi_{1/3}Mn_{1/3}Co_{1/3}O_2$ and proton in water. These refined results almost consistent with results from Wang et al. [26], which revealed that no measurable influence of water on the $LiNi_{0.4}Mn_{1.6}O_4$ crystal structure but a slight lost of Li was found for the pristine material soaked in the water.

A typical SEM image of the $LiNi_{1/3}Mn_{1/3}Co_{1/3}O_2$ particles prepared by the sol–gel method is shown in Fig. 3. Homogeneous $LiNi_{1/3}Mn_{1/3}Co_{1/3}O_2$ particles can be seen in Fig. 3(a). The highly magnified SEM image of $LiNi_{1/3}Mn_{1/3}Co_{1/3}O_2$ shown in Fig. 3(b) indicates its hexagonal morphology, with a particle size range of 100–200 nm.

Table 1
Cell parameters for $LiNi_{1/3}Mn_{1/3}Co_{1/3}O_2$ and $LiNi_{1/3}Mn_{1/3}Co_{1/3}O_2$–CMC soaked in the water.

Sample	*a* (Å)	*c* (Å)	*c*/*a*	*V* (Å^3)	Rw (%)
$LiNi_{1/3}Mn_{1/3}Co_{1/3}O_2$[a]	2.86292(5)	14.25326(7)	4.978	101.1732(1)	6.66
$LiNi_{1/3}Mn_{1/3}Co_{1/3}O_2$[b]	2.87012(1)	14.2798(2)	4.9753	101.873(1)	3.59
$LiNi_{1/3}Mn_{1/3}Co_{1/3}O_2$–CMC-0.5 h[b]	2.87027(1)	14.2789(1)	4.9747	101.876(1)	3.87
$LiNi_{1/3}Mn_{1/3}Co_{1/3}O_2$–CMC-5 h[b]	2.87026(3)	14.2788(0)	4.9747	101.875(1)	3.90
$LiNi_{1/3}Mn_{1/3}Co_{1/3}O_2$–CMC-22 h[b]	2.87003(1)	14.2775(1)	4.9747	101.849(1)	3.38
$LiNi_{1/3}Mn_{1/3}Co_{1/3}O_2$–CMC-48 h[b]	2.87000(2)	14.2775(1)	4.9747	101.848(1)	3.39

[a] Data from XRD refinement.
[b] Data from SXRD refinement from Australian Synchrotron.

Charge–discharge curves of $LiNi_{1/3}Mn_{1/3}Co_{1/3}O_2$ using different binders at various current densities in the voltage range of 2.5–4.6 V are shown in Fig. 4(a–c). The electrochemical behaviour of the $LiNi_{1/3}Mn_{1/3}Co_{1/3}O_2$ materials agrees well with that reported previously [31,33]. The NMC exhibits ~3.75 V charge–discharge voltage plateaus as it experiences the sequential phase transition process ($Ni^{2+} \rightarrow Ni^{3+} \rightarrow Ni^{4+}$). Along with increased charging/discharging current densities, $LiNi_{1/3}Mn_{1/3}Co_{1/3}O_2$ electrode plateaus become shorter and the difference potential (Δ*V*) between the charging and discharging plateaus increase gradually, because of the electrode polarization at high rates. The *dQ*/*dV* curves for $LiNi_{1/3}Mn_{1/3}Co_{1/3}O_2$ with CMC, PVDF, and alginate binders in the potential range of 2.5–4.6 V are presented in Fig. 4(d). The cathodic and anodic peaks of $LiNi_{1/3}Mn_{1/3}Co_{1/3}O_2$ using different binders indicate the potential difference ΔE ($E_{oxidation} - E_{reduction}$) between the oxidation and reduction processes, which correspond to the lithium extraction and insertion, respectively. As a result,

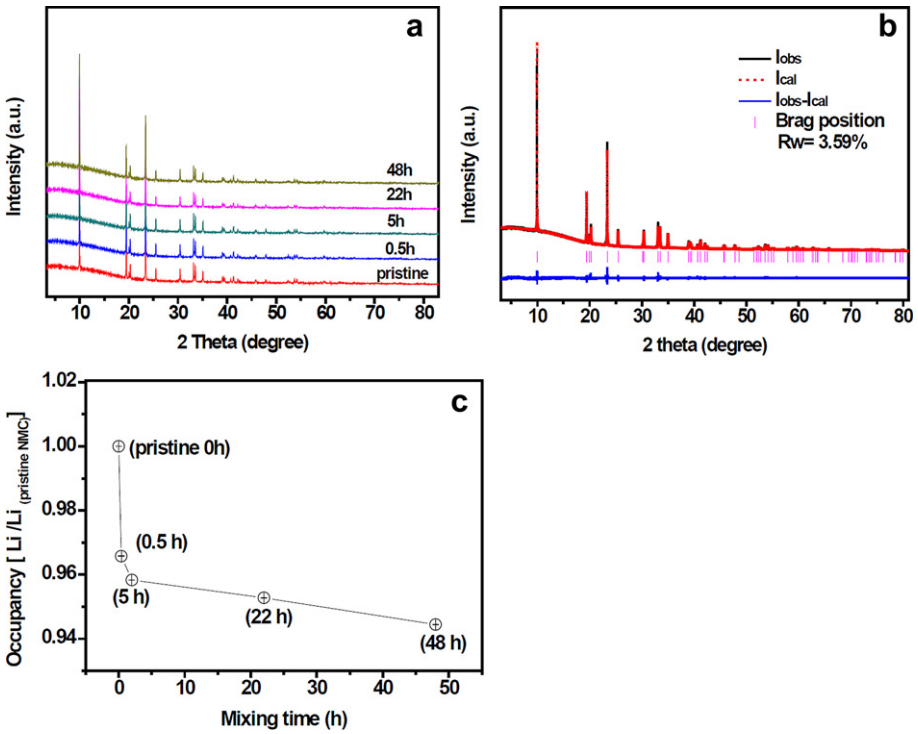

Fig. 2. SXRD patterns (a) $LiNi_{1/3}Mn_{1/3}Co_{1/3}O_2$ mixing with CMC binder in the water for different time; (b) SXRD Rietveld refinement of pristine $LiNi_{1/3}Mn_{1/3}Co_{1/3}O_2$; (c) ratio of $Li/Li_{pristine}$ ($Li_{pristine}$ = 1 for $LiNi_{1/3}Mn_{1/3}Co_{1/3}O_2$) vs. mixing time.

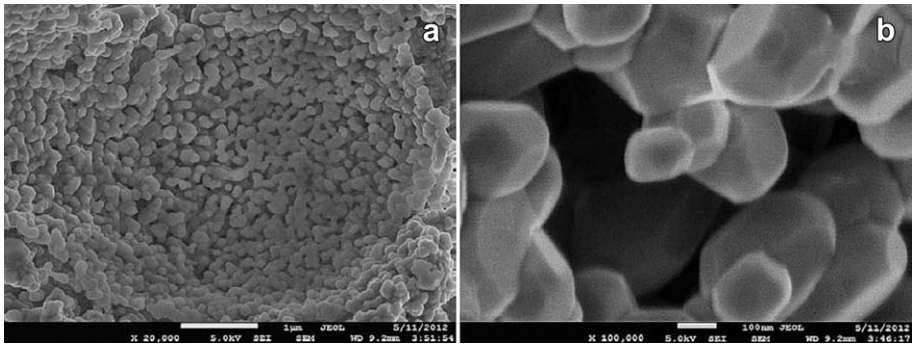

Fig. 3. SEM images of $LiNi_{1/3}Mn_{1/3}Co_{1/3}O_2$ particles: (a) ×20,000; (b) ×100,000.

$LiNi_{1/3}Mn_{1/3}Co_{1/3}O_2$ with PVDF gives a higher cathodic potential of 3.811 V than the electrodes with alginate and CMC binders, with cathodic potentials 3.794 and 3.767 V, respectively. The potential difference ΔE follows the order of CMC (0.0208 V) < alginate (0.096 V) < PVDF (0.101 V) binder, indicating that the electrode using CMC as binder has the lowest electrochemical polarization and the best high rate capability. The lower polarization for $LiNi_{1/3}Mn_{1/3}Co_{1/3}O_2$ using CMC binder could be attributed to the high ionic conductivity of CMC binder in the $LiNi_{1/3}Mn_{1/3}Co_{1/3}O_2$ electrodes [14].

In order to investigate the effects of binders on the rate and cycling performance, $LiNi_{1/3}Mn_{1/3}Co_{1/3}O_2$ cells using different binders were charged and discharged for 105 cycles between 2.5 and 4.6 V at various current densities (Fig. 5), and the current rate was increased from 0.1 to 5 C in steps. As shown in Fig. 5(a), although the $LiNi_{1/3}Mn_{1/3}Co_{1/3}O_2$ cells using PVDF and alginate binders show higher discharge capacity in the initial cycles than that with CMC binder at 0.1 C, the specific capacity measured at the 5 C rate after 100 cycles between 2.5 and 4.6 V was 107.9 mAh g^{-1}, 76.8 mAh g^{-1}, and 8 mAh g^{-1} for $LiNi_{1/3}Mn_{1/3}Co_{1/3}O_2$ using CMC, alginate, and PVDF binder, respectively. The capacity retention for using CMC, alginate, and PVDF binder is 58.5%, 37.4%, and 3.8% of initial capacity after 100 cycles, respectively as shown in Fig. 5(b). Both the cycling performance and the rate capability of the $LiNi_{1/3}Mn_{1/3}Co_{1/3}O_2$ cells with CMC are better than those with alginate or PVDF binder. The reason for dramatically capacity dropping at high C-rates probably could be attributed to the relatively low specific surface area (2.6 m^2 g^{-1}) and the agglomerated big particle size (as shown in Fig. 3) of $LiNi_{1/3}Mn_{1/3}Co_{1/3}O_2$ prepared from sol–gel method [33–35]. The big particle size can limit the lithium intercalation and de-intercalation at high C-rates. Guo et al. [36] reported that $LiNi_{1/3}Mn_{1/3}Co_{1/3}O_2$ prepared by sol–gel method with PVDF binder exhibited nearly no capacity at 6 C. Wang et al. [26] suggested that the CMC as the binder mixed with $LiNi_{0.4}Mn_{1.6}O_2$ material in the water can improve the electronically percolating network. Therefore, we suggest that the CMC and alginate as the binders mixed with $LiNi_{1/3}Mn_{1/3}Co_{1/3}O_2$ material in the water improve the electronically percolating network than that with PVDF binder. The well-define $LiNi_{1/3}Mn_{1/3}Co_{1/3}O_2$ electrode network can be beneficial to enhance the $LiNi_{1/3}Mn_{1/3}Co_{1/3}O_2$ kinetics and then improve the capacity at high C-rates.

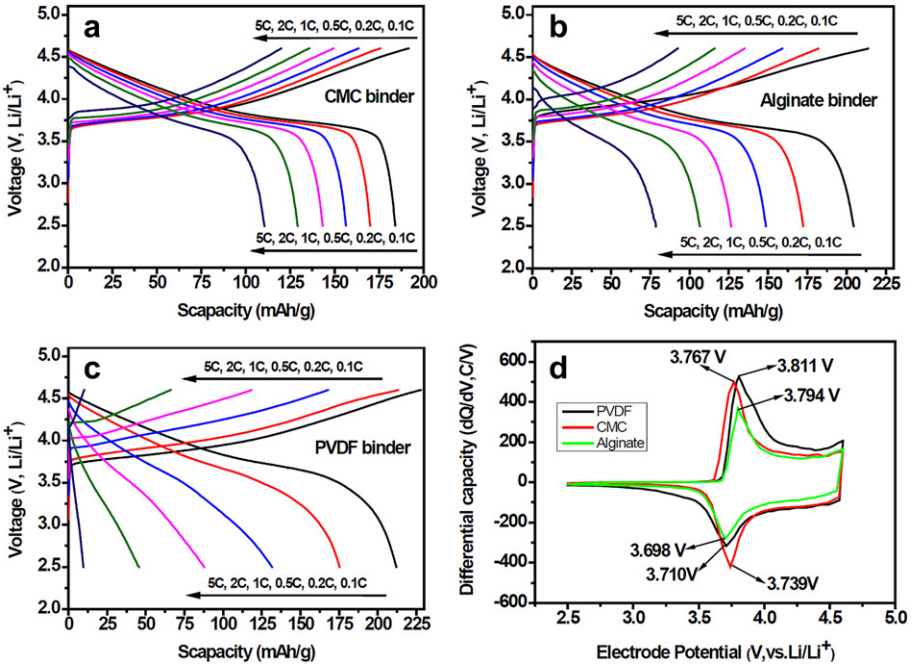

Fig. 4. Initial charge–discharge curves of $LiNi_{1/3}Mn_{1/3}Co_{1/3}O_2$ at various current densities in the voltage range of 2.5–4.6 V using different binders: (a) CMC, (b) alginate, and (c) PVDF; (d) *dQ*/*dV* curves for $LiNi_{1/3}Mn_{1/3}Co_{1/3}O_2$ with CMC, PVDF, and alginate binders.

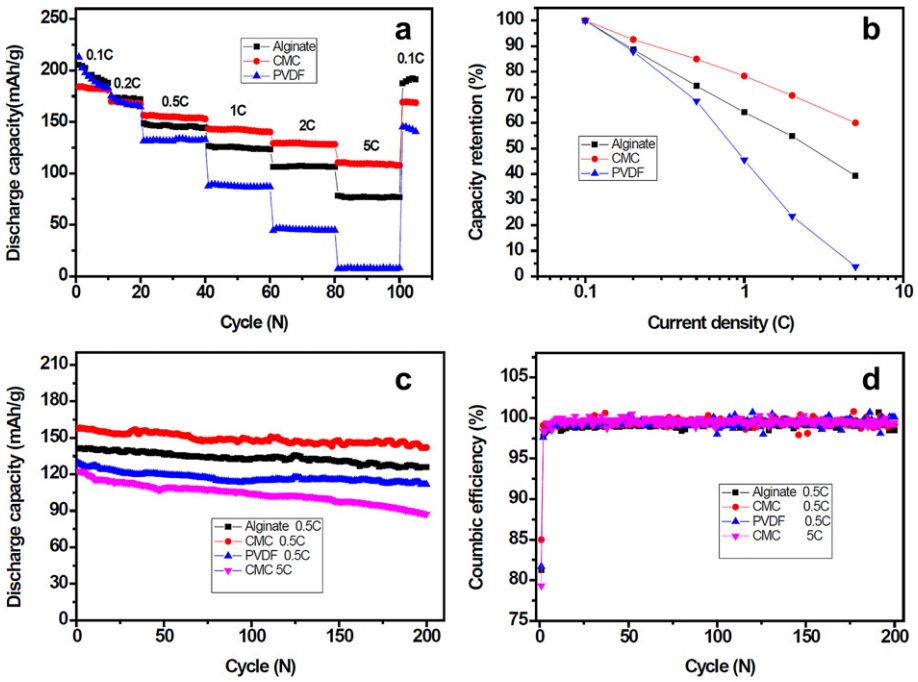

Fig. 5. (a) Rate performance of electrodes; (b) discharge capacity retention at various current densities; (c) cycling performance of $LiNi_{1/3}Mn_{1/3}Co_{1/3}O_2$ with CMC at 0.5 C and 5 C, and with PVDF and alginate at 0.5 C; and (d) coulombic efficiency in the voltage range of 2.5–4.6 V.

In Fig. 5(c and d), the relatively long-term cycling performance and the coulombic efficiency for $LiNi_{1/3}Mn_{1/3}Co_{1/3}O_2$ with different binders are compared at the current densities of 0.5 C and 5 C in the voltage range of 2.5–4.6 V. As shown in Fig. 5(c), the $LiNi_{1/3}Mn_{1/3}Co_{1/3}O_2$ electrode with CMC binder exhibits higher initial discharge capacity, 157.5 mAh g^{-1}, compared to the electrodes with alginate and PVDF binders, 141.1 mAh g^{-1} and 129.3 mAh g^{-1}, respectively. After 200 cycles, discharge capacities of 141.9 mAh g^{-1}, 126 mAh g^{-1}, and 111.7 mAh g^{-1} are obtained at 0.5 C with capacity retention of 90.1%, 89.2%, and 86.3% for $LiNi_{1/3}Mn_{1/3}Co_{1/3}O_2$ with CMC, alginate, and PVDF binder, respectively. Also, the $LiNi_{1/3}Mn_{1/3}Co_{1/3}O_2$ with CMC binder exhibited much higher average discharge capacity of 149.2 mAh g^{-1} compared to ~133.5 mAh g^{-1} for alginate binder and ~117.2 mAh g^{-1} for PVDF binder at 0.5 C after 200 cycles. As shown above in Fig. 5(a), the $LiNi_{1/3}Mn_{1/3}Co_{1/3}O_2$ electrode using CMC binder has the best rate capability at 5 C compared with the other binders. In the long-term cycling, the $LiNi_{1/3}Mn_{1/3}Co_{1/3}O_2$ electrode using CMC binder exhibited the initial discharge capacity of 122.7 mAh g^{-1} with capacity retention of approximately 72.1% over

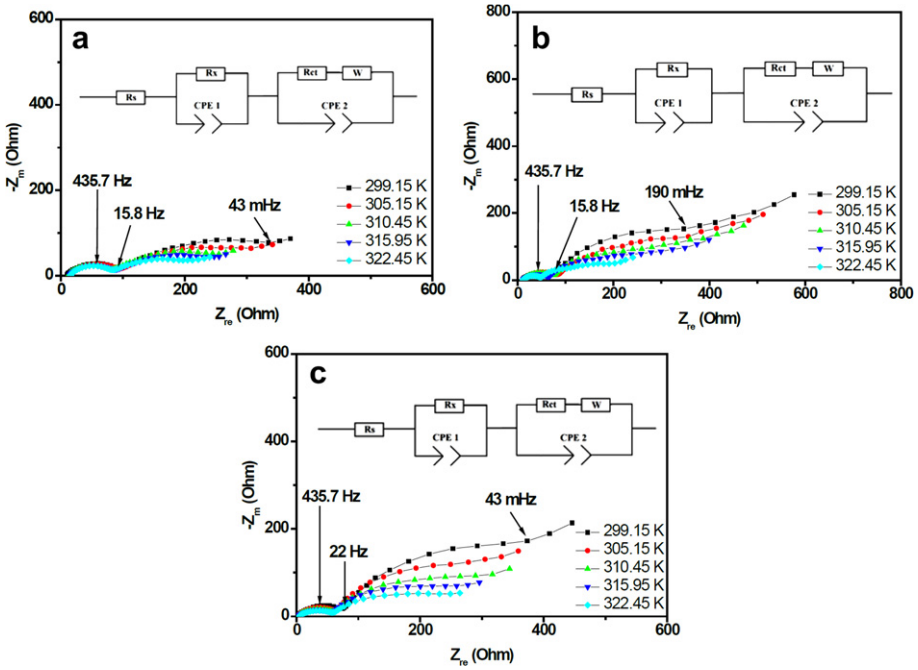

Fig. 6. Nyquist plots of $LiNi_{1/3}Mn_{1/3}Co_{1/3}O_2$ electrodes using CMC (a), alginate (b), and PVDF (c) as binder at the discharged state of 3.70 V (vs. Li/Li^+) at different temperatures and at frequencies from 1 MHz to 10 mHz. The insets show the equivalent circuit.

the 200 cycles at the higher rate of 5 C. The coulombic efficiency was shown in Fig. 5(d). It is worth to mention that $LiNi_{1/3}Mn_{1/3}Co_{1/3}O_2$ with CMC as binder at 0.5 C shows the highest initial coulombic efficiency of 85%. The initial coulombic efficiency for electrodes containing alginate and PVDF binder is 81.7% and 81.3%, respectively. The $LiNi_{1/3}Mn_{1/3}Co_{1/3}O_2$ electrodes using CMC, PVDF, and alginate binder all present high mean coulombic efficiency approaching 99.1% at 0.5 C. Therefore, it can be concluded that the stable layered structured $LiNi_{1/3}Mn_{1/3}Co_{1/3}O_2$ compound presents higher rate capability and cycling performance with CMC binder than with alginate and PVDF binders.

To investigate further the electrode kinetics, the apparent activation energies of $LiNi_{1/3}Mn_{1/3}Co_{1/3}O_2$ electrodes were calculated from electrochemical impedance spectra (EIS). Fig. 6 shows the Nyquist plots of the electrodes with different binders at the discharged state at 3.70 V (vs. Li/Li^+) at different temperatures after charge–discharge for 10 cycles. All the impedance curves of $LiNi_{1/3}Mn_{1/3}Co_{1/3}O_2$ with different binders show two semicircles in the medium frequency and the low frequency regions, which could be assigned to the lithium ion diffusion through the solid electrolyte interphase (SEI) film (R_x) and the charge transfer resistance (R_{ct}), respectively, and an unclear ~45° inclined line in the low-frequency range, which could be considered to be a Warburg impedance. The typical frequencies for the EIS curve at 299.15 K in the two medium and low frequency regions are labelled in Fig. 6. The two semicircles in the medium and low frequency are similar to Guo et al. [36] EIS curves for $LiNi_{1/3}Mn_{1/3}Co_{1/3}O_2$. The R_{ct} is calculated using the equivalent circuit shown in the inset of Fig. 6. The equivalent circuit model also includes electrolyte resistance (R_s), a constant phase element (CPE1) and a non-ideal constant phase element (CPE2). The values of the parameter R_{ct} obtained from a nonlinear least squares fitting are summarized in Table 2. As shown in Table 2, $LiNi_{1/3}Mn_{1/3}Co_{1/3}O_2$ electrode with CMC binder had the smallest R_{ct}, values at different temperatures, below those of alginate binder and PVDF binder, respectively, indicating the enhancement in the kinetics and the consequent improvement in the rate capability of $LiNi_{1/3}Mn_{1/3}Co_{1/3}O_2$ using CMC binder. It should be noted that the ionic conductivity of $LiNi_{1/3}Mn_{1/3}Co_{1/3}O_2$ with different binders increases as the temperature increases from 299.15 K to 322.45 K because of the linear decrease in R_{ct}.

The activation energy of the interface reactions was investigated to understand the kinetics of the charge-transfer reaction [37]. The exchange current (i_0) and the apparent activation energy (E_a) for the lithium intercalated into $LiNi_{1/3}Mn_{1/3}Co_{1/3}O_2$ can be respectively calculated from Equations (1) and (2), the Arrhenius equation.

$$i_0 = RT/(nFR_{ct}) \quad (1)$$

$$i_0 = A\exp(-Ea/RT) \quad (2)$$

where A is a temperature-independent coefficient, R is the gas constant, T (K) is the absolute temperature, n is the number of transferred electrons, and F is the Faraday constant. Fig. 7 shows the

Table 2
Charge transfer resistance R_{ct} for $LiNi_{1/3}Mn_{1/3}Co_{1/3}O_2$ with different binders at various temperatures.

T (K)	Binders		
	CMC	Alginate	PVDF
	$R_{ct}(\Omega)$		
299.15	446.4	574.6	639.6
305.15	372.3	485.6	523.1
310.45	312.2	380.9	416.6
315.95	263.5	308.3	338.8
322.45	218.2	236	240.1

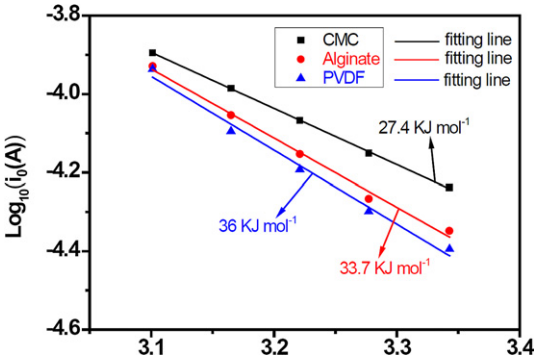

Fig. 7. Arrhenius plots of log i_0 versus $1/T$ for $LiNi_{1/3}Mn_{1/3}Co_{1/3}O_2$ electrodes with CMC, alginate, and PVDF as binder at the discharged state of 3.70 V (vs. Li/Li^+). The lines are the linear fitting results.

Arrhenius plots of log i_0 as a function of $1/T$. The activation energies ($E_a = -Rk$ ln 10, where k = the slope of the fitting line in Fig. 7) of $LiNi_{1/3}Mn_{1/3}Co_{1/3}O_2$ electrodes using CMC, alginate, and PVDF as binder are calculated to be 27.4, 33.7, and 36 kJ mol^{-1}, respectively. These values indicate that $LiNi_{1/3}Mn_{1/3}Co_{1/3}O_2$ with CMC binder shows a lower activation energy for the extraction of lithium ions from the $LiNi_{1/3}Mn_{1/3}Co_{1/3}O_2$ than with alginate and PVDF binders. The lower activation energy of the electrode using CMC as binder facilitates the transport of lithium ions compared with the electrodes with alginate and PVDF as binders, which could be attributed to the higher ionic conductivity of CMC compared with alginate and PVDF.

4. Conclusions

$LiNi_{1/3}Mn_{1/3}Co_{1/3}O_2$ cathode material having uniform and clear crystalline morphology, with a particle size range of 100–200 nm, was successfully prepared by the sol–gel method. The electrochemical results revealed that, although the $LiNi_{1/3}Mn_{1/3}Co_{1/3}O_2$ electrodes blended with ~5% PVDF and alginate binders presented higher discharge capacity at low rate (0.1 C) than the electrode using CMC binder, the $LiNi_{1/3}Mn_{1/3}Co_{1/3}O_2$ electrode blended with CMC binder presented better cycling performance and rate capability than those with alginate and PVDF binders. EIS test results indicated that the $LiNi_{1/3}Mn_{1/3}Co_{1/3}O_2$ electrode using CMC as binder had much lower charge transfer resistance and lower activation energy than the electrodes using alginate and PVDF as the binders. The electrochemical performance results indicate that the cheap and environmental friendly CMC as a binder for $LiNi_{1/3}Mn_{1/3}Co_{1/3}O_2$ can improve the high rate capability and reduce the cost of lithium ion batteries in comparison with current commercial PVDF binder.

Acknowledgements

Financial support provided by the Australian Research Council (ARC) through discovery project (DP110103909) is acknowledged. The authors also want to thank Dr. T. Silver for critical reading of the manuscript. Part of experiment was performed at Powder Diffraction beamline at Australian Synchrotron.

References

[1] M. Park, X.C. Zhang, M.D. Chung, G.B. Less, A.M. Sastry, J. Power Sources 195 (2010) 7904–7929.
[2] D.R. Rolison, R.W. Long, J.C. Lytle, A.E. Fischer, C.P. Rhodes, T.M. McEvoy, M.E. Bourga, A.M. Lubers, Chem. Soc. Rev. 38 (2009) 226–252.
[3] J.C. Guo, C.S. Wang, Chem. Commun. 46 (2010) 1428–1430.
[4] G. Liu, S.D. Xun, N. Vukmirovic, X.Y. Song, P. Olalde-Velasco, H.H. Zheng, V.S. Battaglia, L.W. Wang, W.L. Yang, Adv. Mater. 23 (2011) 4679–4683.

[5] D.Y. Wang, S.E. Ela, S.M. Zakeeruddin, P. Pechy, I. Exnarc, Q. Wang, M. Gratzel, Electrochem. Commun. 11 (2009) 1350–1352.
[6] P. Biensan, B. Simon, J.P. Pérès, A. De Guibert, M. Broussely, J.M. Bodet, F. Perton, J. Power Sources 81–82 (1999) 906–912.
[7] S.F. Lux, F. Schappacher, A. Balducci, S. Passerini, M. Winter, J. Electrochem. Soc. 157 (2010) A320–A325.
[8] M. He, L.X. Yuan, W.X. Zhang, X.L. Hu, Y.H. Huang, J. Phys. Chem. C 115 (2011) 15703–15709.
[9] H. Buqa, M. Holzapfel, F. Krumeich, C. Veit, P. Novák, J. Power Sources 161 (2006) 617–622.
[10] L. El Ouatani, R. Dedryvere, J.B. Ledeuil, C. Siret, P. Biensan, J. Desbrieres, D. Gonbeau, J. Power Sources 189 (2009) 72–80.
[11] G.T. Kim, S.S. Jeong, M. Joost, E. Rocca, M. Winter, S. Passerini, A. Balducci, J. Power Sources 196 (2011) 2187–2194.
[12] I. Kovalenko, B. Zdyrko, A. Magasinski, B. Hertzberg, Z. Milicev, R. Burtovyy, I. Luzinov, G. Yushin, Science 333 (2011) 75–79.
[13] A. Sano, M. Kurihara, K. Ogawa, T. Iijima, S. Maruyama, J. Power Sources 192 (2009) 703–707.
[14] S.L. Chou, J.Z. Wang, H.K. Liu, S.X. Dou, J. Phys. Chem. C 115 (2011) 16220–16227.
[15] S.L. Chou, J.Z. Wang, C. Zhong, M.M. Rahman, H.K. Liu, S.X. Dou, Electrochim. Acta 54 (2009) 7519–7524.
[16] J. Li, H.M. Dahn, L.J. Krause, D.-B. Le, J.R. Dahn, J. Electrochem. Soc. 155 (2008) A812–A816.
[17] D. Munao, J.W.M. van Erven, M. Valvo, E. Garcia-Tamayo, E.M. Kelder, J. Power Sources 196 (2011) 6695–6702.
[18] N. Ding, J. Xu, Y.X. Yao, G. Wegner, I. Lieberwirth, C.H. Chen, J. Power Sources 192 (2009) 644–651.
[19] J. Li, R.B. Lewis, J.R. Dahn, Electrochem. Solid State Lett. 10 (2007) A17–A20.
[20] N.S. Hochgatterer, M.R. Schweiger, S. Koller, P.R. Raimann, T. Wohrle, C. Wurm, M. Winter, Electrochem. Solid State Lett. 11 (2008) A76–A80.
[21] J.S. Bridel, T. Azais, M. Morcrette, J.M. Tarascon, D. Larcher, Chem. Mater. 22 (2010) 1229–1241.
[22] A. Guerfi, M. Kaneko, M. Petitclerc, M. Mori, K. Zaghib, J. Power Sources 163 (2007) 1047–1052.
[23] J.H. Lee, J.S. Kim, Y.C. Kim, D.S. Zang, U. Paik, Ultramicroscopy 108 (2008) 1256–1259.
[24] J.H. Lee, H.H. Kim, S.B. Wee, U. Paik, Kona: Powder Part. J. (2009) 239–245.
[25] J. Li, R. Klopsch, S. Nowak, M. Kunze, M. Winter, S. Passerini, J. Power Sources 196 (2011) 7687–7691.
[26] Z.L. Wang, N. Dupre, A.C. Gaillot, B. Lestriez, J.F. Martin, L. Daniel, S. Patoux, D. Guyomard, Electrochim. Acta 62 (2012) 77–83.
[27] B.J. Hwang, Y.W. Tsai, D. Carlier, G. Ceder, Chem. Mater. 15 (2003) 3676–3682.
[28] N. Yabuuchi, Y. Koyama, N. Nakayama, T. Ohzuku, J. Electrochem. Soc. 152 (2005) A1434–A1440.
[29] Z. Wang, Y. Sun, L. Chen, X. Huang, J. Electrochem. Soc. 151 (2004) A914–A921.
[30] K.M. Shaju, P.G. Bruce, Adv. Mater. 18 (2006) 2330–2334.
[31] T. Ohzuku, K. Ariyoshi, S. Yamamoto, Y. Makimura, Chem. Lett. 30 (2001) 1270–1271.
[32] N. Yabuuchi, T. Ohzuku, J. Power Sources 119–121 (2003) 171–174.
[33] Z.-D. Huang, X.-M. Liu, S.-W. Oh, B. Zhang, P.-C. Ma, J.-K. Kim, J. Mater. Chem. 21 (2011) 10777–10784.
[34] C.-H. Lu, B.-J. Shen, J. Alloys Compd. 497 (2010) 159–165.
[35] X.-M. Liu, W.-L. Gao, B.-M. Ji, J. Sol-Gel Sci. Technol. 61 (2012) 56–61.
[36] K.-C. Jiang, S. Xin, J.-S. Lee, J. Kim, X.-L. Xiao, Y.-G. Guo, Phys. Chem. Chem. Phys. 14 (2012) 2934–2939.
[37] Y. Yamada, Y. Iriyama, T. Abe, Z. Ogumi, J. Electrochem. Soc. 157 (2010) A26–A30.